ADVANCED FUNCTIONAL MATERIALS
www.afm-journal.de

Light-Powered Healing of a Wearable Electrical Conductor

Hong Suk Kang, Hee-Tak Kim, Jung-Ki Park,* and Seungwoo Lee**

Mechanical failure along a conductive pathway can cause unexpected shutdown of an electronic devices, ultimately limiting the device lifetime. To address this problem, various systems to realize healable electrical conductors have been proposed; however, rapid, noninvasive, and on-demand healing, factors that are all synergistically required, especially for wearable device applications, still remains challenging. Here, a light-powered healable electrical conductor (conceptualized as photofluidic diffusional system) is proposed for simple-, fast-, and easy-to-implement wearable devices (e.g., the electronic skin, sensitive to mechanical motion). Contrary to other implementations such as capsules, heat, water, and mechanical forces, green light even with low intensity has potential to provide fast (less than 3 min) and repetitive recovery of a damaged electrical conductor without any direct invasion. Also, the multiple, irregular cracks resulting from vigorous motions of wearable devices can be simultaneously recovered regardless of the light incident angles and crack propagation directions, thus, making light-powered healing more accessible to wearable devices beyond existing system options. To develop and demonstrate the key concepts of this system, combined studies on materials, integrations, and light-powering strategy for recovering a damaged wearable electrical conductor are systematically carried out in the present work.

1. Introduction

As electronic devices have become more complex and highly integrated, just one small failure (e.g., physical disconnections from accidental cracks or operational fatigue) along the electrical conductive pathway can render the entire device useless.[1–6] In particular, wearable electronic devices, which inevitably undergo dynamic and vigorous motions (e.g., bending, folding, or twisting), are much more liable to suffer from such conductive failures, compared with conventional flat electronic devices.[7–9] Thus, recovery from conductive failure even in recently advanced wearable electronic devices has emerged as a challenging issue. Healable electrical conductors, wherein a conductivity failure can be autonomically or non-autonomically repaired via an internal or external trigger, offer a potentially promising solution to the central challenge of conductive failures within electronic devices. Upon this background, a variety of systems to develop healable electric conductors have been intensively explored.[10–17] They can be categorized into three main groups: i) two-layered, composite systems (i.e., spreading conductive materials onto various healable polymers including a Diels-Alder reaction-based healable polymer[10] and a water-enabled healable polymer[11]; ii) organometallic systems in which conductive metal ions or metallic microparticles are homogeneously dispersed within a supramolecular (e.g., hydrogen-bond) polymeric network;[12,13] and iii) micro-capsule or pipeline systems with the liquid metals that can be autonomically released and penetrated into the broken conductive pathways.[14–17] Although these systems offer efficient recovery of the electrical conductive property (≈90%), the stimuli for non-autonomic healing such as heat at high temperature (>110 °C),[10] water,[11] and mechanical pressure[12] can cause additional damages to the electronic devices, and a metallic micro-capsule or pipeline system[14–17] is unable to provide a repeated restoration of conductive failures. Especially, these disadvantages of existing system options limit their availability of wearable device applications, which require a repeatable, ambient, rapid, and noninvasively remote healing process. Developing a robust healing platform particularly for wearable devices thus remains a challenge.

In this paper, we propose a generic non-autonomic healing system, a light-powered, healable electrical conductor, in order to overcome the aforementioned challenges. The use of light as an external stimulus rather than the other implements applied in the previously suggested systems has potential to provide a remote access to the restoration of its conductivity without a direct invasion of the master device, which can cause additional device failures. Light-enabled, noninvasive healing of an electrical conductor thus enhances process safety and facilitates

H. S. Kang, Prof. J.-K. Park
Graduate School of EEWS
Korea Advanced Institute of Science and Technology (KAIST)
Daejeon 305–701, Korea
E-mail: jungpark@kaist.ac.kr
Prof. H.-T. Kim, Prof. J.-K. Park
Department of Chemical and Biomolecular Engineering
Korea Advanced Institute of Science and Technology (KAIST)
Daejeon 305–701, Korea
E-mail: heetak.kim@kaist.ac.kr
Prof. S. Lee
SKKU Advanced Institute of Nanotechnology (SAINT)
& School of Chemical Engineering
Sungkyunkwan University (SKKU)
Suwon 440–746, Korea
E-mail: seungwoo@skku.edu

DOI: 10.1002/adfm.201401666

on-demand treatment so as to allow amendable platform for healing of wearable devices such as the electronic skin.

Light-powered healing is implemented in the present work via use of a photochromic soft material (i.e., an azobenzene material), which can be directionally diffused along the light polarization.[18–33] This unique directionality of the material diffusion with respect to light polarization enables an efficient healing process regardless of crack propagation directions, light incident angles, and the number of cracks. Furthermore, thanks to the high quantum yield of azobenzene,[18] which is used in this work as photochromic molecule, directional molecular diffusion even with low light intensity (at room temperature) is achieved in a fast (within a few minutes) and repeatable (several times) manner. By depositing silver nanowires (AgNWs, conducting material used in this study) onto the top layer of the flexible photochromic soft material, we extend this optically healable material to have fully functional electrical conductivity. Notably, AgNWs were found to maintain conformable contact with the photochromic soft material even during the diffusible optical healing process. Thus, herein, AgNWs and the photochromic soft material act as conductive pathways and a light-powered cargo carrier, respectively; the synergetic effect detailed from combining these various advantages provides rapid, noninvasive, and on-demand healing for a flexible electronic conductor, making light-powered healing more amenable to dynamically deformable wearable devices beyond existing systems. While structural recovery of materials by using light as a stimulus has been explored previously,[34–37] here we further extend the concept to build up light-powered healing of wearable electronic devices.

2. Results and Discussion

2.1. Light-Powered, Structural Healing by Directional Photofluidization

The azobenzene material used in this study is an epoxy-based amorphous polymer, poly(disperse orange) 3 (PDO 3, Mw ≈ 4700, PDI: 1.74, and T_g: 120 °C); the chemical structure is shown in **Figure 1**a. The azobenzene material exhibits a unique and fascinating phenomenon known as athermal directional photofluidization.[18–33] When light with an absorption wavelength (herein 532 nm) is irradiated onto the azobenzene material (i.e., PDO 3, azobenzene polymer, abbreviated as azopolymer), the photochromic azobenzene molecules grafted to the main chain undergo a repetitive photoisomerization between trans- and cis-isomers until the long axis of the azobenzene molecules is perfectly aligned in a direction perpendicular to the incident light polarization (see Figure 1b). Interestingly, such repeated photoisomerization gives rise to the anisotropic bulk diffusion of the azopolymer even under the glass transition temperature (T_g) or melting temperature (T_m).[18–33] Notably, as shown in Figure 1c (scanning electron microscope, SEM), a square post of PDO 3 (20 μm × 20 μm × 11 μm), developed by soft-imprinting, was reconfigured into specific shapes even at room temperature, according to the light polarization: the pristine square was elongated in the direction of the light polarization (Figure 1d,e) and transformed into a isotropic dome by the irradiation of a circularly polarized light (Figure 1f). In particular, the distinct rectangular post became a rounded dome under light irradiation owing to the tendency to minimize surface tension. This is strong evidence of PDO 3's fluidic behavior by light irradiation at room temperature. These exotic behaviors clarify that the diffusion of azobenzene material originates solely from photo-induced molecular motions and the resultant athermal photofluidization at room temperature (not photo-thermal effect).

Then, we investigated the light-powered, structural healing capability of the azobenzene material through light irradiation onto a crack generated in PDO 3 film: the detailed procedure for the preparation of the PDO 3 film (5 μm thickness) onto a 70 μm thick polyethylene terephthalate film (PET) film is described in the Experimental Section. We introduced a 15 μm wide and 5 μm deep crack onto the PDO 3 film using a cutting knife and irradiated the *s*-polarized electrical field of light, perpendicular to the crack propagation direction in the PDO 3 film. Light is irradiated in the backside direction (see optical setup described in Figure S1, Supporting Information). The intensity employed in this study was 600 mW/cm^2; the threshold intensity for photofluidization was empirically determined as 5 μW/cm^2. The distribution of the time-averaged, electric-field intensity (E^2) within the 5 μm thick PDO 3 film was numerically simulated by the finite-domain, time-difference (FDTD) method, as shown in Figure 1g (also see Figure S2, Supporting Information). The electric-field intensity (E^2) gradually decreased along the PDO 3 film thickness; however, intensity of a few μW/cm^2 (beyond the threshold intensity for photofluidization) is still survived at the end of the PDO 3 film. As a result, photofluidic diffusion of the entire PDO 3 can occur effectively, even if the velocity of diffusion should vary along the PDO 3 film thickness. SEM images in Figure 1h demonstrate the representative recovery kinetics of the 15 μm wide and 5 μm deep crack in PDO 3 through photofluidic diffusion; indeed, light irradiation for only 120 s achieved full recovery of the crack in the PDO 3 film. Significantly, the huge edge roughness that is inevitably formed during the mechanical cutting step (Figure 1h) was completely smoothed out after light-powered healing. This is because the transition of the initially solid PDO 3 to a fluid state together with its directional diffusion tends to minimize the surface area of the PDO 3 film. The full restoration of the crack in PDO 3 was completed in a relatively short period (120 s); however, the required healing time by light irradiation could vary, according to the PDO 3 thickness, light intensity, and light polarization. In particular, we tested the dependence of light-powered healing kinetics on the angle between the polarization and crack propagation direction. For example, as the linear polarization of light is deviated from *s*-polarized light, the required healing time was increased (Figure S3, Supporting Information); the initial crack width remained almost unchanged even after prolonged exposure (150 s) of *p*-polarized light, parallel to the crack propagation direction (Figure S4, Supporting Information). This strong dependence of healing kinetics to light polarization further provides evidence of directional photofluidic diffusion of the azobenzene material (Figures S3–4, Supporting Information). However, we can still observe the phenomenon of photofluidic smoothing of the huge edge roughness resulting

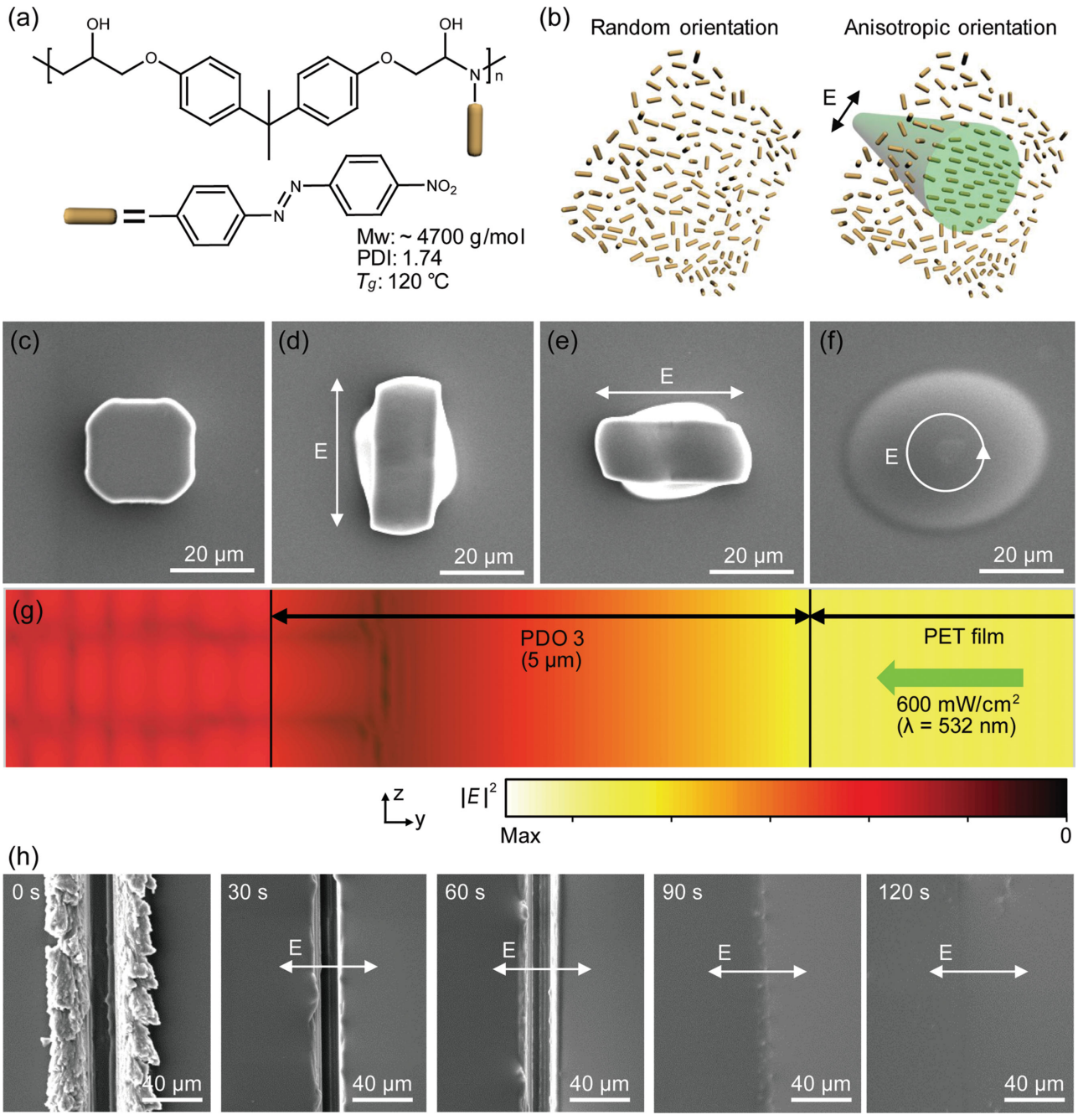

Figure 1. Light-powered structural healing of damaged azobenzene material: a) Chemical structure of polydisperse orange 3 (PDO 3, azobenzene material used in this work). The orange rod indicates the azobenzene molecular moiety attached to the polymeric backbone. b) Schematic diagram showing the anisotropic molecular alignment of azobenzene molecules by light irradiation: the long-axis of azobenzene can be aligned in the direction perpendicular to the light polarization. Top-view scanning electron microscope (SEM) images of (c) pristine and photo-reconfigured PDO 3 posts by d) vertically linear polarization, e) horizontally linear polarization, and f) left-handed circular polarization. g) Simulated, time-averaged electric-field (E^2) distribution within the PDO 3 layer along the *y*–*z* plane. h) SEM images taken at various stages of light-powered (*s*-polarization) healing of linearly cracked PDO 3 film (15 μm width and 5 μm depth).

from mechanical cutting (see Figure S4b, Supporting Information). Meanwhile, the irradiation of circularly polarized light leads to full restoration of the same crack; the required healing time with application of circular-polarized light irradiation, however, is slightly longer (150 s) compared with the case of *s*-polarized light irradiation, as shown in Figure S4, Supporting Information. This is because the photofluidic diffusion by circular-polarized light irradiation was radially induced instead of the linear photofluidic diffusion by *s*-polarized light irradiation. Conclusively, the data above reveal the strong feasibility of azobenzene materials as a general class of structural healing materials.

2.2. Light-Powered, Non-Invasive Healing of an Electrical Conductor

We next extended the light-powered, healable azobenzene material to have fully functional, electrical properties through large-area, uniform deposition of AgNWs onto PDO 3, as presented in **Figure 2**a,b. By using a polyol reduction process,[38–40] AgNWs with average diameter of 150 nm and length of 15 μm were massively synthesized; the synthesized AgNWs subsequently were deposited on the large-area PDO 3/PET film by an electrostatic spray process (the home-built facility in Figure 2a was used with the condition described in Table S1, Supporting Information). Figure 2c–e (also see Figure S5a,b, Supporting Information) present the conformably deposited AgNW mesh on the PDO 3 film (averaged number of AgNW mesh layer and their surface coverage ratio were 5 and 30%, respectively). The resistance of this flat AgNW mesh/PDO 3 film without any mechanical deformation was 6.1 Ω (2 cm length and 1 cm width). This excellent conductivity of the layered film resulted from well-developed wire-wire junctions together with enough density. Interestingly, the resistance of the layered AgNW mesh/PDO 3 film varied from 4.7 Ω to 19 Ω (the fractional change defined by $(R - R_0)/R_0$ (%) in the resistance varied from –23% to +216%), as the flexion angle (4 nm radius curvature) was changed in both the forward (increasing θ) and backward (decreasing θ) directions (see Figure 2f and Movie clip S1, Supporting Information). The compressive and tensile strains at the AgNW mesh are spontaneously generated, when the layered AgNW mesh/PDO 3 film is uniaxially bended with negative and positive flexion angles. Therefore, the strength of the wire-wire junctions becomes sensitive to the bending motion, and the fractional change in the resistance of the layered AgNW mesh/PDO 3 is reduced (for compressive strain) or enhanced (for tensile strain). It is also important to note that the resistance of the layered AgNW mesh/PDO 3 was more sensitive to tensile strain rather than compressive strain. This is because the initially well-developed wire-wire junction with high density is more difficult to be further compressed than relaxed. This apparent trend of the resistance sensitivity to bending motion can be similarly driven by torsional motion (twisting with 4 nm radius curvature): the fractional change in the resistance of the layered AgNW mesh/PDO 3 varied from –21% (for compressive strain) and to +242% (for tensile strain), as summarized in Figure 2g. Therefore, this flexible AgNW mesh/PDO 3 provides potential to electronic skin with the capability for mechanical motion sensing. Also, even at extremely high flexion or torsion angle (≈170°) with 4 nm radius curvature, the layered film still showed sufficient electrical conductivity (resistance is as low as 30 Ω) for lighting a white light-emitting diode (LED) bulb (see Figure 2h and Movie clip S1–2, Supporting Information). Indeed, we did not observe any delamination of AgNWs from the PDO 3 film when the layered film was bended or twisted even at ≈170° of flexion or torsion angle, respectively, as presented in Figure S6, Supporting Information. More importantly, the wire-wire junctions can withstand during 500 iterations of bending or twisting/relaxing cycles, as evidenced by the nearly unchanged resistance (see Figure 2i). The excellent mechanical compliance, flexibility, and durability of the AgNW mesh/PDO 3 layered conductor were attributed to three main factors: i) the high flexibility of the mechanically durable PDO 3/PET film (measured modulus of 4879 MPa, Figure S7, Supporting Information); ii) strong adhesion in the wire-wire junction; and iii) the AgNW mesh's strong adhesion (91 nN) to the PDO 3 layer (Figure S8a, Supporting Information). This unique layered electrical conductor system thus holds promise for flexible/wearable device applications.

Next, we verified that the layered AgNW mesh/PDO 3 film has the ability to heal conductive failure (i.e., cracks) as well as structural damage merely by light irradiation. The key to success for light-powered healing of this conductor is that PDO 3 can convey the AgNW layer during its photofluidic directional diffusion (light-powered cargo carrier). We performed an experiment involving mechanical cutting and light-powered healing of a layered AgNW mesh/PDO 3 film, as summarized in **Figure 3**a–f (SEM images of Figure 3a–c and dark-field optical microscope images of Figure 3d–f): in false-color SEM images (Figure 3a–c), PDO 3 is highlighted in orange (high-magnified false-color SEM image is presented in Figure S9, Supporting Information). The mechanical cutting of the layered AgNW mesh/PDO 3 conductor with a knife generated a 15 μm wide and 5 μm deep crack (see the SEM image in Figure 3b and the dark-field optical microscope image in Figure 3e). The *s*-polarized light, perpendicular to the direction of crack propagation, was exposed on the backside, as light irradiated at the front side is inevitably scattered by the AgNW mesh and distributed non-uniformly within the PDO 3 film (see optical simulation results of Figure 3g,h and Figure S10, Supporting Information). As clearly shown in Figure 3c (SEM image) and Figure 3f (dark-field optical microscope image), the previously formed 15 μm wide crack was structurally restored after irradiation of the *s*-polarized light for 120 s. More importantly, the in situ photodiffusion of the AgNW mesh was directly visualized by a dark-field optical microscope combined with a laser light source (see Figure S11, Supporting Information). A series of dark-field optical microscope images (before cracking: Figure 3d, after cracking: Figure 3e, and after healing: Figure 3f) and Movie clip S3 of Supporting Information obviously reveal the movement of the AgNW mesh along with photofluidic diffusion of PDO 3. This direct visualization of the AgNW mesh movement further confirms that PDO 3 indeed acts as a light-powered cargo carrier for healing electrical conductivity by taking advantage of the increased work of adhesion between them during light irradiation (from 91 nN to 557 nN, see Figure S8b). We additionally observed that the AgNW mesh is partially penetrated into the recovered region of the PDO 3 layer, as a result of photofluidic softening (see Figure 3c, Figure S9, and Figure S12, Supporting Information); thus, the somewhat darker line in the dark-field optical microscope image (Figure 3f) is still visible after full-structural recovery.

To quantitatively evaluate the ability of the mechanically damaged AgNW mesh/PDO 3 film to heal its electrical conductivity by light, the measurement of the resistance variation during the cracking and healing process was carried out in real-time (see Figure 3i). We clearly observed that the dramatically increased resistance (2.8×10^8 Ω, open-circuit) can almost be returned to its original value of ≈15.1 Ω, as presented in Figure 3i. In this case, it took 120 s to almost recover the initial electrical conductivity; this is comparable to the time required

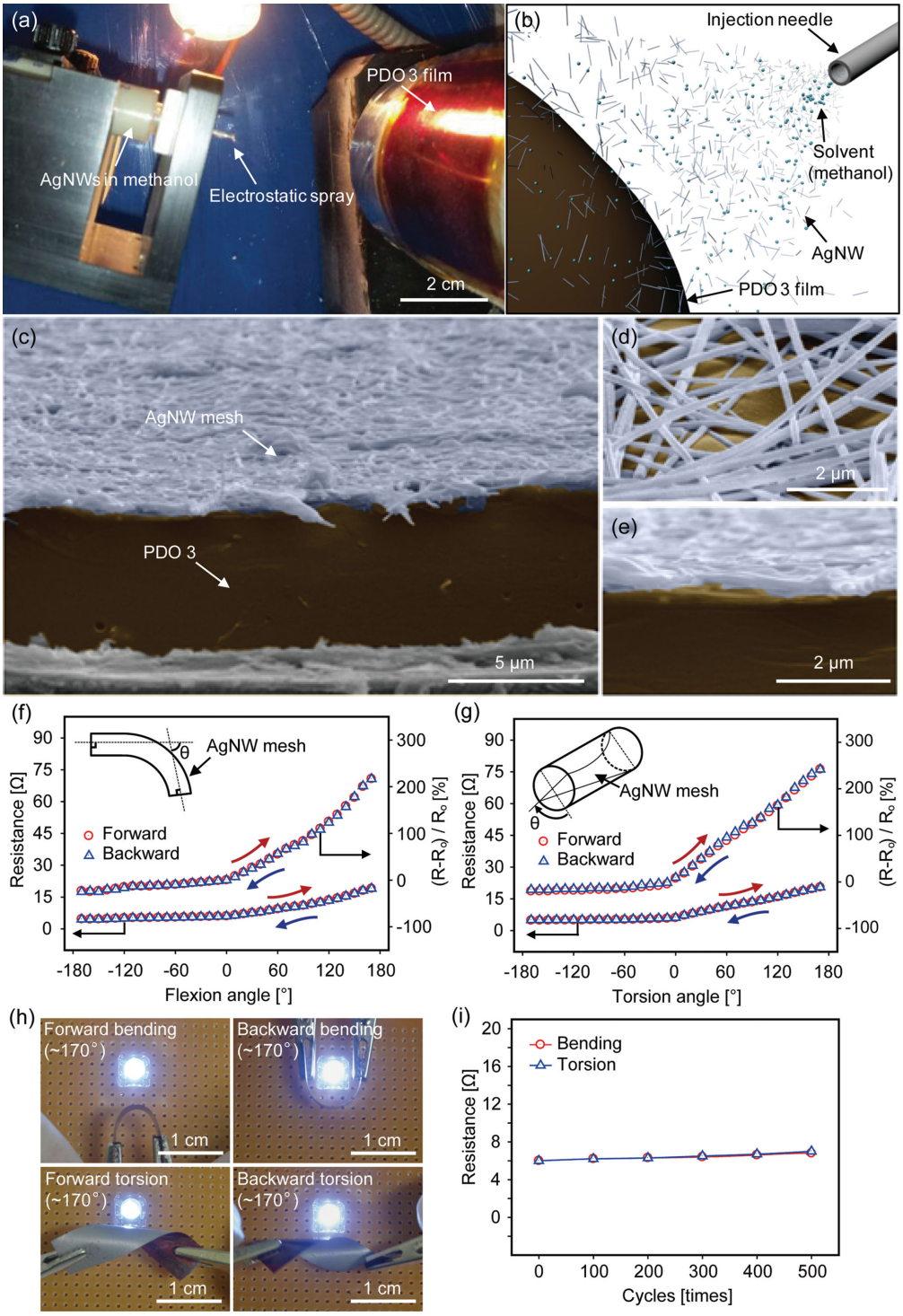

Figure 2. Layered silver nanowire (AgNW) mesh/PDO 3 film as a flexible electrical conductor/skin sensitive to mechanical motions: a) Photograph of the home-built facility enabling uniform deposition of AgNWs onto PDO 3 film. b) Schematic diagram of AgNW mesh electrostatically jetted from the needle. False-color SEM images of layered AgNW mesh/PDO 3 film with c) low-magnified, perspective-view, d) high-magnified, top-view, and e) high-magnified, cross-sectional view. PDO 3 and the AgNW mesh are highlighted in orange and light blue, respectively. Plot of mechanical motion-dependent change in resistance, during f) bending and g) twisting of the AgNW mesh/PDO 3 layered film. As flexion and torsion angle is increased from –170° to + 170°, the resistance is continuously enhanced. This is because the tensile stress is additionally generated at the AgNWs mesh side. (h) Photographs showing lighting white light emitting diode (LED) bulb connected with layered AgNW mesh/PDO 3 film bended (two images in top panel) or twisted (two images in bottom panel) at high angles (± 170°). High electrical conductivity enough to turn on the white LED bulb can be still maintained even at the extreme flexion or torsion angles. i) Plot illustrating the change in the resistance of the layered AgNW mesh/PDO 3 film with the number of mechanical distortions (i.e., bending or twisting/relaxation cycles).

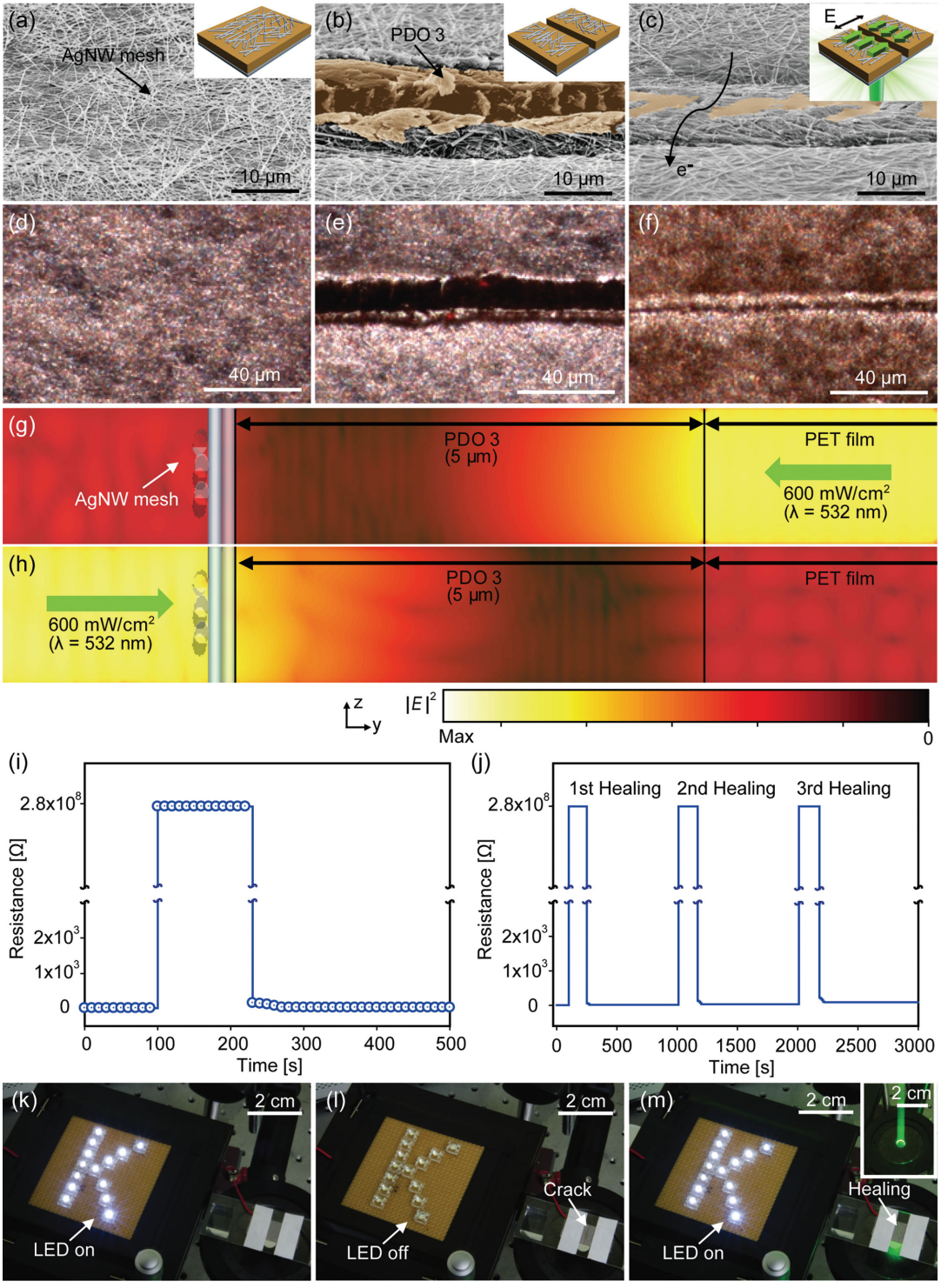

Figure 3. Demonstration system for light-powered healing of electrical conductor: Perspective-view SEM images of a) pristine, b) cracked, and c) optically-healed AgNW mesh/PDO 3 layered film. The dimensions of the generated crack were 15 μm width and 5 μm depth. Top-view dark-field optical microscope images of d) pristine, e) cracked, and f) optically-healed AgNW mesh/PDO 3 layered film. The many differently colored, bright dots or lines indicate the AgNW mesh. Simulated, time-averaged electric-field (E^2) distribution within AgNW mesh/PDO 3 layered film along the *y*–*z* plane, when the light is irradiated in the g) backward and h) forward directions. i) Plot of the transient resistance behavior demonstrating kinetics of light-powered healing of the cracked AgNW mesh/PDO 3 layered film. j) Repeatability of light-powered healing of three cuts at the same area of the AgNW mesh/PDO 3 layered film. Images illustrating the cracking-optical healing sequence of AgNW mesh/PDO 3-connected white LED bulb pattern with a "K" geometry corresponding to the k) initial stage, l) cracking stage, and m) fully recovered stage. The inset of (m) indicates the irradiation of light with 532 nm wavelength through the hole of the sample holder (the diameter of incident light is about 5 mm).

for structural healing of the PDO 3 crack without AgNW mesh. Indeed, the broken wire-wire junctions were well recovered, as shown in Figure 13Sa, Supporting Information. The data indicate that the AgNW mesh does not significantly affect the photofluidic diffusion of PDO 3, as long as the light is irradiated on the backside to minimize the scattering effect. We also observed that light irradiation on the front side does not readily trigger overall photofluidic diffusion of the layered film owing in part to the scattering-induced, non-uniform distribution of electric-field intensity ($|E^2|$) within the PDO 3 film and in part to randomized light polarization.

Repeated healing capability is of critical importance for a practical application to functional wearable devices.[10–12] To investigate the repeatability of our healing process, mechanical cutting and subsequent light-powered healing were repeated at the same location; the associated resistance variation of the AgNW mesh/PDO 3 layered conductor during the repeated cutting-healing process is presented in Figure 3j. After each cutting, the resistance dramatically increased to 2.8×10^8 Ω; the recoverable resistance, after three iterations of mechanical cutting/light-powered healing at the same area, gradually increased from 15.1 Ω (1st healing) to 90.2 Ω (3rd healing). The enhanced recovered resistance with cycles of mechanical cutting and light-powered healing is attributed to the full embedment of the AgNW mesh into the PDO 3 film (see Figure 3c and Figure S13b, Supporting Information) and the resultant weakening of the wire-wire junction: the photofluidic softening helps PDO 3 penetrate the AgNW junctions, consequently resulting in significantly weakened AgNW junctions after three times iterations of the light-powered healing process. However, this enhanced recoverable resistance with the number of healing cycles could be further mitigated with optimization of the light penetration depth or the use of conductive particles homogeneously dispersed in the healing material (composite system).[12,13]

By connecting the layered AgNW mesh/PDO 3 with a white LED bulb in a circuit, the conductivity healing can be visually verified, as shown in images of Figure 3k–m. The detailed experimental setup and healing procedure related to the LED circuit healing test are shown in Figure S14 and Movie clip S4, Supporting Information. The LED bulb pattern with a "K" geometry connected in a parallel relation (a turn-on voltage of 2.5 V) was lit with a DC voltage of 3.0 V. After mechanically cutting of the AgNW mesh/PDO 3 conductor, the LED went off (Figure 3l). When the light was exposed on the damaged conductive pathway (see light exposure presented in the inset of Figure 3m), the LED bulb suddenly lit up at the exposure time of ≈110 s (Figure 3 m).

The final step in checking the feasibility of light-implementation with a healing of electrical conductor was to access whether the optically recovered AgNW mesh/PDO 3 layered film can be durable in terms of electrical properties. To do this, we investigated two key determinants for electrical durability of the healed AgNW mesh/PDO 3: the resistance variation with the number of bending/twisting cycles (**Figure 4**a) and the change in transient resistance sensitivity to bending or twisting with the number of healing process (Figure 4b,c). As with the pristine AgNW mesh/PDO 3, there are no significant losses in electrical conductivity with the number of bending/twisting cycles of the AgNW mesh/PDO 3 that was healed several times, as presented in Figure 4a. Moreover, the fractional change in the resistance to mechanical motions (bending and twisting) did not varied significantly even during three iterations of light-powered healing, as shown in Figure 4b–d (resistance plot and LED lighting during bending/twisting of the layered AgNW mesh/PDO 3 healed one- or three-time). These results imply that both the electrical durability with the number of mechanical motions and the resistance sensitivity to mechanical motions maintained unchanged even after several iterations of light-powered healing, such that the layered AgNW mesh/PDO 3 film has potential to be used as light-powered healable electronic skin.

2.3. Light-Powered Healing Platform for Wearable Electronic Devices

For wearable device applications, it should be possible to accomplish simultaneous healing of multiple, irregular cracks even on a curvilinear substrate, which could be accidentally caused by vigorous motions (e.g., folding, wrinkling, and twisting) with an on-demand and non-invasive treatment. In line with this, we extended the light-powered healing process of a single crack on a flat electrical conductor, which is conceptualized as photofluidic directional diffusion of AgNW mesh, to on-demand healing of multiple cracks on a curved substrate (a representative non-flat substrate).

The first step in this direction is to exploit the recovery kinetics of the crack in the AgNW mesh/PDO 3 with different incident angles of light (see **Figure 5**a). For wearable devices, the electrical conductor could be subjected to a curvilinear or twisted geometry; the recovery of the broken-electrical pathway consequently should be achieved regardless of the light incident angle. Figure 5b,c show the recovery kinetics and required healing time, determined by the transient period of resistance values from 2.8×10^8 Ω to ≈15.1 Ω, as a function of the light incident angle. The apparent trend was that for a single crack in the layered AgNW mesh/PDO 3 film (15 μm width and 5 μm depth), the required healing time varied from ≈120 s to ≈150 s, as the light incident angle increased from 0° (normal) to 80 °. This slightly increased healing time with the light incident angle mainly originated from enhanced reflection of the slanted incident light from the surface of the PET substrate. However, the full recovery of the damaged electrical pathway was still achieved in a relatively fast manner (150 s) even at an extremely high incident angle (i.e., 80°). This is because the light polarization impinged on the PDO 3/PET film was not changed significantly with respect to the different incident angles.

The capability of simultaneous healing of multiple, irregular cracks was next investigated under the same optical experimental conditions. We arbitrary generated two irregular cracks with different propagation directions, shapes, and widths (ranged from 14 μm to 18 μm) by using a cutting knife and simultaneously healed these irregular cracks by the linearly polarized light irradiation in a normal direction (the light polarization is dictated in Figure 5d). As shown in Figure 5d, a series of dark-field optical microscope images taken before and after

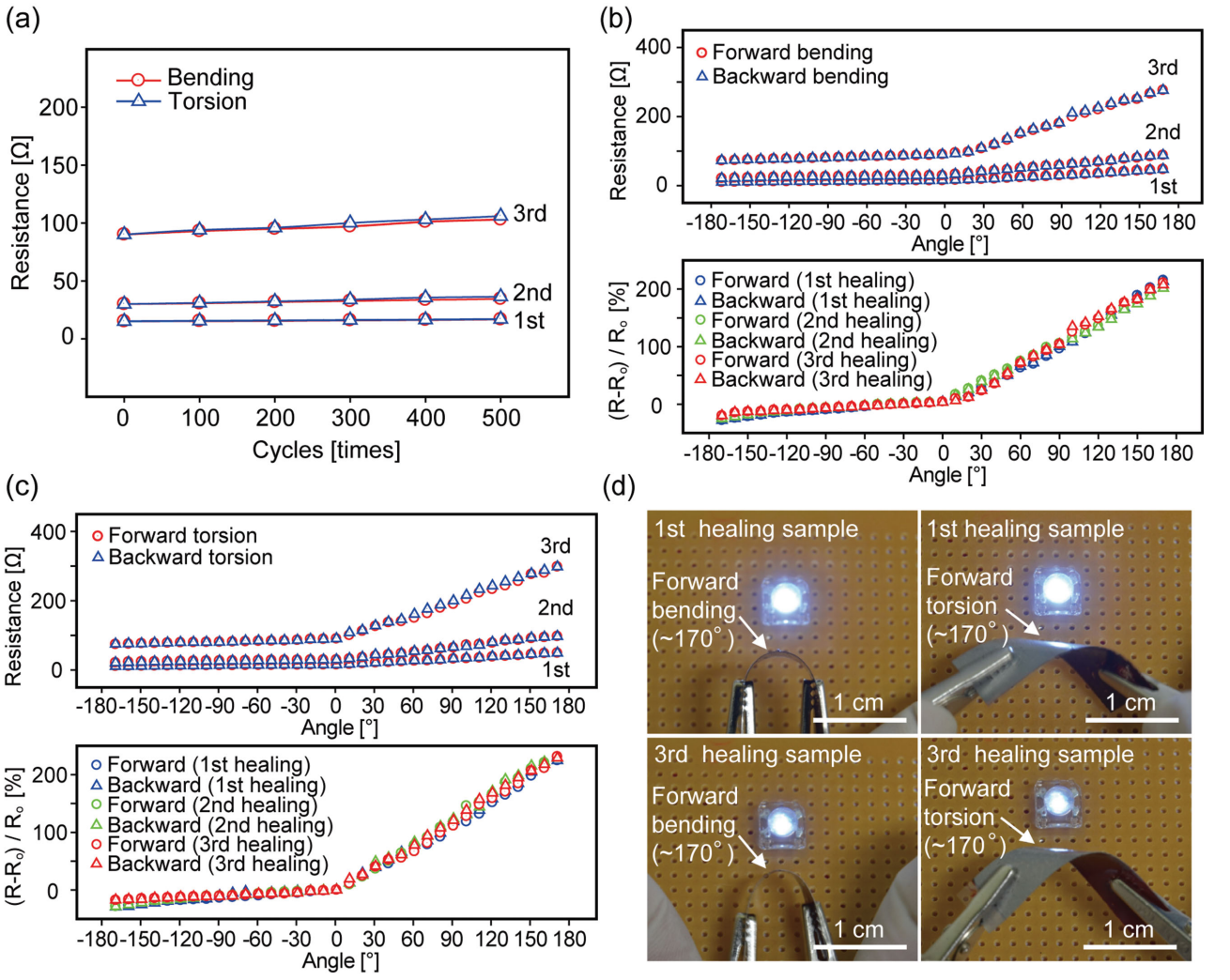

Figure 4. Electrical characteristics of optically healed AgNW mesh/PDO 3 film: a) Representative durability of electrical properties of AgNW mesh/PDO 3 film with the number of optical healing. The resistance was measured after different cycles of bending or twisting/relaxing. Typical resistance sensitivity of several times optically healed AgNW mesh/PDO 3 film to b) bending and c) twisting motions. d) Photographs showing lighting of white LED bulb connected to the bended or twisted AgNW mesh/PDO 3 films which are one-time (two images in top panel) and three-time (two images in bottom panel) optically healed. The left and right columns in both top and bottom panels correspond to forward bending and twisting, respectively.

the light irradiation clearly shows simultaneous recovery of these irregular cracks. This recovery of multiple broken-electrical pathways by directional photofluidic diffusion was further evidenced by the restoration of resistance (see Figure 5e). However, it is important to note that the required healing time of these irregular multiple cracks with different propagation directions, shapes, and widths was distinctly increased (≈350 s), compared with that of a single crack, while simultaneously the recovered resistance was also further increased (180 Ω). These significantly increased healing time and recovered resistance are mainly due to the non-parallelized crack propagation directions (both cracks are not perpendicular to the light polarization), different crack width (required healing time is proportional to the crack width, as shown in Figure S15, Supporting Information), and the increased the number of cracks to be healed.

The on-demand healing process of the layered AgNW mesh/PDO 3 film equipped on the hand (the outside of the forefinger) of an Iron Man toy, as displayed in **Figure 6**, demonstrates the generality of our light-powered approach in the recovery of a wearable electronic conductor. Figure 6a,b present the layout for wiring a white LED bulb with the layered AgNW mesh/PDO 3 on the Iron Man hand: the white line box in Figure 6b presents the layered AgNW mesh/PDO 3, while the white LED bulb is incorporated into the palm of Iron Man toy hand. The conductive pathway in wearable electronic devices may more frequently undergo mechanical damage caused by film distortions including bending, folding, and twisting induced by vigorous motion. For example, during bending of the forefinger of the Iron Man hand (see Figure 6c), exceeding the modulus of the AgNW mesh/PDO 3 conductor at a certain level of strain actually resulted in the generation of two irregular cracks (randomly distributed width, shape, and propagation direction, as presented in Figure 6d,e and Movie clip S5, Supporting Information) and the white LED turned off (Figure 6f,g). These two

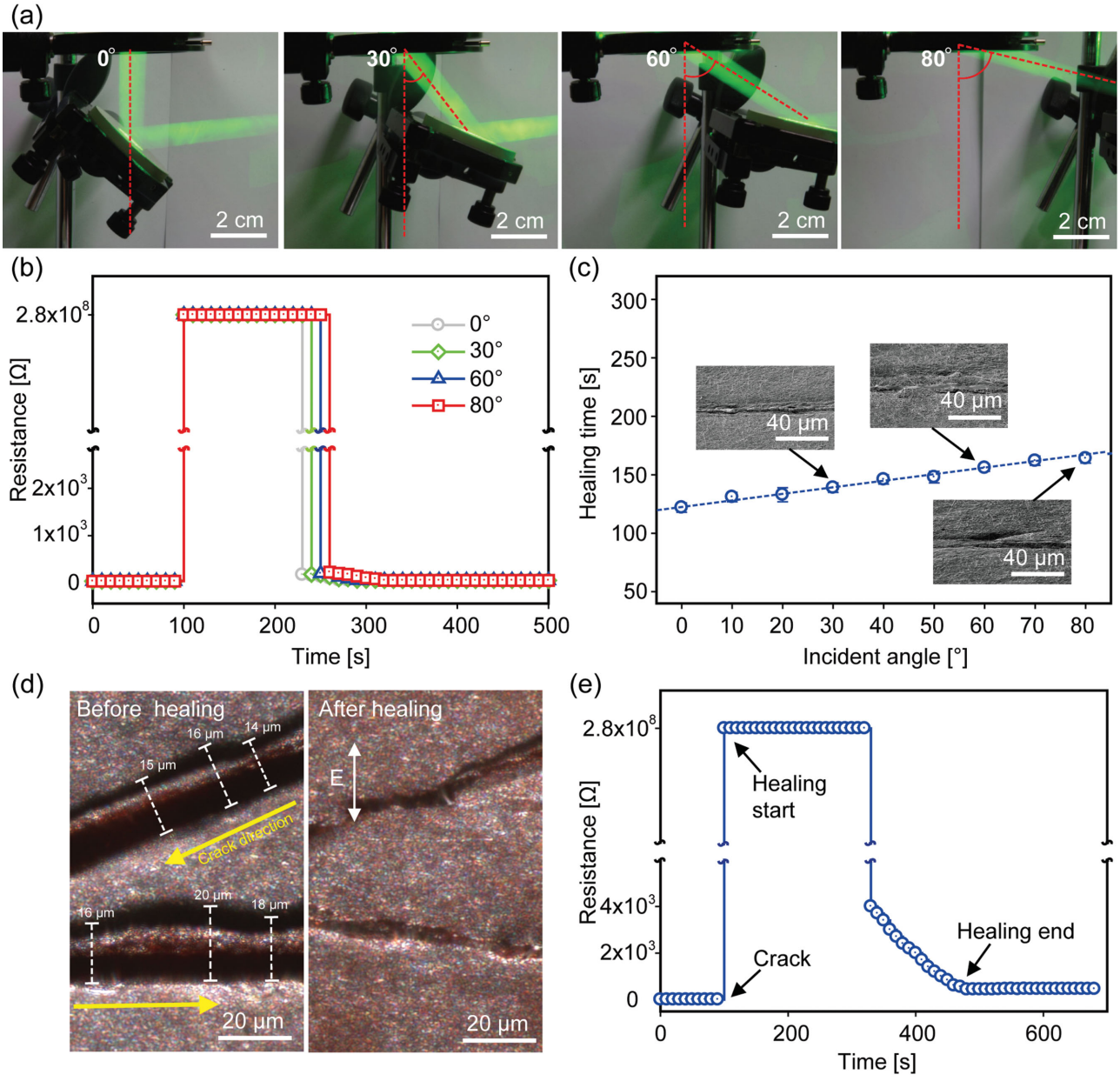

Figure 5. Light-powered healing of a single crack regardless of incident angles and simultaneous healing of two cracks with different propagation directions: a) Images presenting light irradiation with different incident angles. Experimental results of b) light-powered healing kinetics of a single crack (15 μm width and 5 μm depth) in AgNW mesh/PDO 3 as a function of light incident angles and c) the required healing time defined by the retention time at resistance of 2.8×10^8 Ω (open-circuit). The insets of (c) present SEM images taken after healing of single crack with the different light incident angles (30°, 60°, and 80°). Light-powered, simultaneous healing of two irregular cracks with different propagation directions (highlighted by yellow arrows) characterized by d) dark-field optical microscope images and e) plot presenting the resistance transition with light irradiation time.

irregular cracks on the curvilinear surface can be simultaneously recovered by the irradiation of a single linearly polarized light (see the polarization dictated in Figure 6e) within 400 s (LED lit again as presented in Figure 6h); the data show that this approach enables the recovery of the multiple irregular cracks regardless of the incident angle of the light. It is also important to note that the light can be locally irradiated onto the damaged forefinger of the Iron Man toy so as to heal the electrical conductor without direct invasion to other areas (see more details about on-demand light-powered healing of electrical conductor in Figure S16, Supporting Information). Thus, this experiment demonstrates the ability of light-powered healing as a versatile and general platform for the recovery of a damaged wearable electronic conductor.

3. Conclusions

Light-powered healing of electrical conductor should greatly expand the range of its possible applications with enhanced

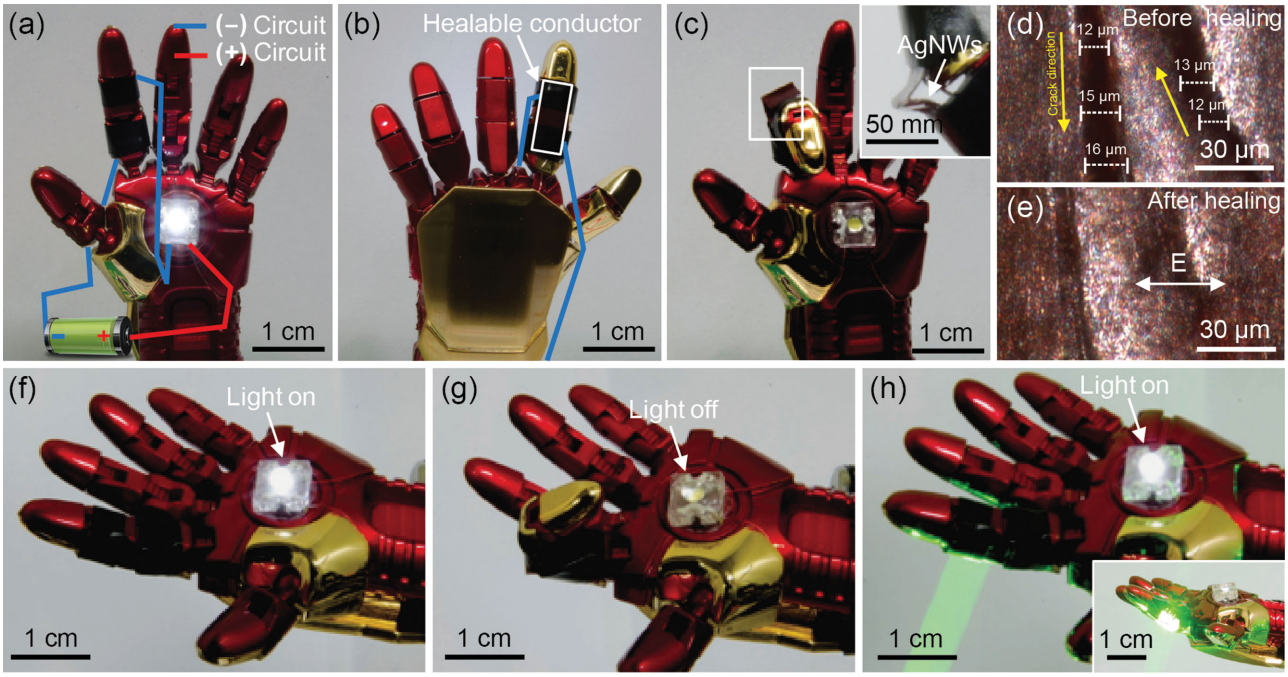

Figure 6. Demonstration platform for the generality of light-powered healing of a wearable electrical device: Images showing the circuit layout of wiring a white LED (on the palm of the hand of an Iron Man toy) with the AgNW mesh/PDO 3 layered film taken at a) front side and b) backside views. The white box in (b) indicates the layered AgNW mesh/PDO 3 film attached onto the forefinger of the Iron Man hand; the AgNW mesh is located at the inner side. c) Image of bended (spreading forefinger) and relaxed (bending forefinger) AgNW mesh/PDO 3 layered film. The inset image presents a cross-sectional view showing the bended AgNW mesh/PDO 3 layered film when the bended forefinger is relaxed. Dark-field optical microscope images of d) two different irregular cracks with different propagation directions (highlighted by yellow arrows) and e) optically recovered two irregular cracks in a curved AgNW mesh/PDO 3 layered film. Two irregular cracks were simultaneously generated when the AgNW mesh/PDO 3 layered film exceeds its modulus by vigorous bending motion. f–h) Perspective-view images illustrating the generality of light-powered healing of a damaged wearable electric conductor. f–g) The pristine AgNW mesh/PDO 3 layered film connected with a white LED was damaged (LED went off) with two different cracks. h) The two irregular cracks generated on the curved AgNW mesh/PDO 3 layered film (d) by bending at a level exceeding film's modulus were simultaneously healed (LED turned on again) by slanted light irradiation.

on-demand, non-invasive stimuli, which is not accessible by other methods. Directional photofluidic diffusion of an AgNW mesh/azobenzene material, which is newly conceived in the present work, generalizes the basic concept of light-powered healing to remote restoration of multiple irregular cracks on curvilinear substrate so as to enable wearable devices applications. Regardless of the incident angle of the light, light-powered healing of multiple irregular cracks on a flexible conductor can be accomplished as little as a few minutes. Improvement in the repeatability of light-powered healing will be critical to enable robust applications of realistic wearable electronic devices. Potential works in this direction include further optimization of the number of AgNW mesh layer and PDO 3 thickness, incorporation of a passivation layer onto PDO 3 to prevent the embedment of AgNW mesh into PDO 3, and homogeneously mixing electrical conducting components with PDO 3 instead of the current two-layered system.

4. Experimental Section

Preparation of poly(disperse orange 3) (PDO 3): The PDO 3 was obtained by solid-state step polymerization of disperse orange 3 (5.8 mmol, Sigma-Aldrich) and bisphenol A diglycidyl ether (5.8 mmol, Sigma-Aldrich). The reaction temperature and time were 110 °C and 2 days, respectively. After the reaction, the PDO 3 was dissolved by 50 mL of tetrahydrofuran (THF, Sigma-Aldrich); then, this PDO 3 dispersed in THF was precipitated by dropwise adding 500 mL methanol. After following vacuum filtration, the final PDO 3 was dried in vacuum oven at 100 °C for 3 days in order to completely remove the solvent. The weight-average molecular weight and the polydispersity index (PDI) of the synthesized PDO 3 were 4700 g/mol and 1.74, respectively. The glass transition temperature (T_g) of PDO 3 was 120 °C.

Preparation of PDO 3 Film: 5 μm thick PDO 3 film was prepared by solvent-assisted drop and spin casting method. The synthesized PDO 3 was firstly dissolved in cyclohexanone (Sigma-Aldrich) with 30%; then, we carefully dropped this PDO 3 solution onto the polyethylene terephthalate (PET) substrate. PET substrate had already been cleaned by a series of deionized water, acetone, and ethanol washing; subsequently treated with oxygen plasma in order to improve its surface wettability with cyclohexanone. The PDO 3 drop onto PET substrate was then casted by spinning at 200 rpm for 300 s. When cyclohexanone was completely evaporated at 45 °C for 12 h, the 5 μm thick PDO 3 layer onto PET substrate was uniformly obtained.

Synthesis of AgNW: Silver nanowires (AgNWs) were synthesized by a solution method known as the polyol process.[38–40] We first added 1.336 g of polyvinylpyrrolidone (PVP, Mw ≈ 55 000, powder, Sigma-Aldrich) to 20 mL of ethylene glycol (EG, Sigma-Aldrich) in round-bottom flask and stirred this mixture at 200 rpm by using a magnetic stirrer. The mixture was then heated up to 170 °C; the 0.1 g of finely grounded silver chloride (AgCl, Sigma-Aldrich) was subsequently added into the flask for the initial nucleation of the silver seeds. After 6 h stirring, 0.44 g of silver nitrate ($AgNO_3$,

Sigma-Aldrich) is gradually added into the solution for 30 min. The main reason of this gradual addition of $AgNO_3$ is to prevent the synthesis of other shaped Ag nanostructures (e.g., spheres, cubes, or rods). After three times washing by consecutive process composed of spinning (at 6000 rpm for 30 min), removing residual chemicals (e.g., EG, PVP, and other impurities), and re-dispersing precipitated AgNWs, the purified AgNWs (Figure S5, Supporting Information) dispersed in methanol were obtained.

Preparation of AgNW Mesh/PDO 3 Film: AgNWs was uniformly deposited onto 5 μm thick PDO 3 layer by the electrostatic spraying. Especially, by the electrostatic spraying of AgNWs-dispersed methanol solution (20 mg/mL) onto the PDO 3 film (Figure 2a), the mesh geometry with conformable wire-wire junction can be generated over the large area.[40] The detail conditions for electrostatic spraying of AgNWs-dispersed methanol solution are described in Table S1, Supporting Information.

Optical Simulation Details: The numerical simulations of electric-field intensity (E^2) distributions within pure PDO 3 layer and AgNW mesh/PDO 3 double layer, which are demonstrated in the manuscript and the Supporting Information (Figure 1g, 3g, 3h, S2, and S7), were carried out by using a commercially available finite-difference, time-domain (FDTD) so ftware package (FDTD solutions 8.7, Lumerical). For all calculations, the complex permittivity of Ag and the refractive index of PDO 3 were empirically obtained by using ellipsometry (EP3, Nanofilm); the meshed cubit unit cell of the simulated model along all directions has 80 nm (for PDO 3) or 15 nm (for AgNW mesh/PDO 3) in size. The geometry of AgNW mesh, presented in Figure S10a-b of Supporting Information is partially taken from the representative SEM image in Figure S5b, Supporting Information.

Optical Setup: The detailed light irradiation setup for optical healing is presented in Figure S1 and Figure S14, Supporting Information. The intensity and wavelength of the laser light source (Opto Engine LLC, 3 W) were 600 mW/cm^2 and 532 nm, respectively. The intensity of the beam was precisely adjusted by using a neutral density (ND) filter and the polarization of beam was controlled by adjusting the director of wave plate. By using a spatial filter, the initial beam with Gaussian intensity profile was converted into the plane beam with uniform intensity profile. The set of lens and spatial filter allows us to enlarge the beam diameter from 1 mm to 1 cm; the final beam size was further controlled by using iris. The light irradiation time was precisely controlled by an electronic shutter.

Characterizations: The images demonstrating i) structural features of the layered AgNW mesh/PDO 3, ii) light-powered healing kinetics, iii) white light emitting diode (LED) circuit, and iv) optical setup were obtained by using field-emission scanning electron microscopy (FE-SEM, FEI, Sirion), dark field optical microscopy (Olympus, BX51), and digital camera (Canon, EOS 50D). The resistance measurements were performed by using Fluke 187 multimeters (two point probe measurement, Fluke Corp.).

Supporting Information

Supporting Information is available from the Wiley Online Library or from the author.

Acknowledgements

This research was supported by the Basic Science Research Program through the National Research Foundation of Korea (NRF) funded by the Ministry of Education, Science, and Technology (code# NRF-2012R1A1A2042558), WCU program (EEWS) at KAIST (code# R-31–2008–000–1005–0), the Pioneering Nano-Based Convergence HRD Center (BK21+ program at Sungkyunkwan University), and the 8th National Core Research Center at Sungkyunkwan University (Center for Human Interface Nano Technology, HINT), which is funded by the NRF of the Korean Government (MSIP) (No. 2009-0083540). The Acknowledgements were updated on December 10, 2014.

Received: May 23, 2014
Revised: August 14, 2014
Published online: September 15, 2014

[1] D.-H. Kim, J. Xiao, J. Song, Y. Huang, J. A. Rogers, *Adv. Mater.* **2010**, *22*, 2108.
[2] S. C. B. Mannsfeld, B. C.-K. Tee, R. M. Stoltenberg, C. V. H.-H. Chen, S. Barman, B. V. O. Muir, A. N. Sokolov, C. Reese, Z. Bao, *Nat. Mater.* **2010**, *9*, 859.
[3] P. Lee, J. Lee, H. Lee, J. Yeo, S. Hong, K. H. Nam, D. Lee, S. S. Lee, S. H. Ko, *Adv. Mater.* **2012**, *24*, 3326.
[4] T. Sekitani, T. Someya. *Adv. Mater.* **2010**, *22*, 2228.
[5] L. Hu, M. Pasta, F. L. Mantia, L. Cui, S. Jeong, H. D. Deshazer, J. W. Choi, S. M. Han, Y. Cui, *Nano Lett.* **2010**, *10*, 708.
[6] C. Yan, J. Wang, X. Wang, W. Kang, M. Cui, C. Y. Foo, P. S. Lee, *Adv. Mater.* **2014**, *26*, 943.
[7] U. N. Maiti, J. Lim, K. E. Lee, W. J. Lee, S. O. Kim, *Adv. Mater.* **2014**, *26*, 615.
[8] J. Y. Kim, B. H. Kim, J. O. Hwang, S.-J. Jeong, D. O. Shin, J. H. Mun, Y. J. Choi, H. M. Jin, S. O. Kim, *Adv. Mater.* **2013**, *25*, 1331.
[9] S. K. Hwang, J. M. Lee, S. Kim, J. S. Park, H. I. Park, C. W. Ahn, K. J. Lee, T. Lee, S. O. Kim, *Nano Lett.* **2012**, *12*, 2217.
[10] C. Gong, J. Liang, W. Hu, X. Niu, S. Ma, H. T. Hahn, Q. Pei, *Adv. Mater.* **2013**, *25*, 4186.
[11] Y. Li, S. Chen, M. Wu, J. Sun, *Adv. Mater.* **2012**, *24*, 4578.
[12] B. C.-K. Tee, C. Wang, R. Allen, Z. Bao, *Nat. Nanotechnol.* **2012**, *7*, 825.
[13] K. A. Williams, A. J. Boydston, C. W. Bielawski, *J. R. Soc. Interface* **2007**, *4*, 359.
[14] S. R. White, N. R. Sottos, P. H. Geubelle, J. S. Moore, M. R. Kessler, S. R. Sriram, E. N. Brown, S. Viswanathan, *Nature* **2001**, *409*, 794.
[15] B. J. Blaiszik, S. L. B. Kramer, M. E. Grady, D. A. McIlroy, J. S. Moore, N. R. Sottos, S. R. White, *Adv. Mater.* **2012**, *24*, 398.
[16] S. A. Odom, S. Chayanupatkul, B. J. Blaiszik, O. Zhao, A. C. Jackson, P. V. Braun, N. R. Sottos, S. R. White, J. S. Moore, *Adv. Mater.* **2012**, *24*, 2578.
[17] B. J. Blaiszik, S. L. B. Kramer, S. C. Olugebefola, J. S. Moore, N. R. Sottos, S. R. White, *Annu. Rev. Mater. Res.* **2010**, *40*, 179.
[18] R. H. El Halabieh, O. Mermut, C. J. Barrett, *Pure Appl. Chem.* **2004**, *76*, 1445.
[19] H. S. Kang, S. Lee, S.-A. Lee, J.-K. Park, *Adv. Mater.* **2013**, *25*, 5490.
[20] G. J. Fang, J. E. Naclennan, Y. Yi, M. A. Glaser, M. Farrow, E. Korblova, D. M. Walba, T. E. Furtak, N. A. Clark. *Nat. Commun.* **2013**, *4*, 1521.
[21] A. Ambrosio, L. Marrucci, F. Borbone, A. Roviello, P. Maddalena, *Nat. Commun.* **2012**, *3*, 989.
[22] P. Karageorgiev, D. Neher, B. Schultz, B. Stiller, U. Pietsch, M. Giersig, L. Brehmer, *Nat. Mater.* **2005**, *4*, 699.
[23] S. Lee, J. Shin, H. S. Kang, Y.-H. Lee, J.-K. Park, *Adv. Mater.* **2011**, *23*, 3244.
[24] S. Lee, J. Shin, Y.-H. Lee, S. Fan, J.-K. Park, *Nano Lett.* **2010**, *10*, 296.
[25] H. Yu, T. Ikeda, *Adv. Mater.* **2011**, *23*, 2149.
[26] S. Lee, H. S. Kang, J.-K. Park, *Adv. Mater.* **2012**, *24*, 2069.
[27] H. S. Kang, S. Lee, J.-K. Park, *Adv. Funct. Mater.* **2011**, *21*, 4412.
[28] D. Wang, G. Ye, X. Wang, X. Wang, *Adv. Mater.* **2011**, *23*, 1122.
[29] S. Lee, H. S. Kang, J.-K. Park, *Adv. Funct. Mater.* **2011**, *21*, 1770.
[30] C. J. Barrett, A. L. Natansohn, P. Rochon, *J. Phys. Chem.* **1996**, *100*, 8836.
[31] A. Priimagi, M. Saccone, G. Cavallo, A. Shishido, T. Pilati, P. Metrangolo, G. Resnati, *Adv. Mater.* **2012**, *24*, OP345.
[32] O. Kulikovska, L. M. Goldenberg, L. Kulikovsky, J. Stumpe, *Chem. Mater.* **2008**, *20*, 3528.
[33] I. Ishow, R. Camacho-Aguilera, J. Guérin, A. Brosseau, K. Nakatani, *Adv. Funct. Mater.* **2009**, *19*, 796.
[34] M. Burnworth, L. Tang, J. R. Kumpfer, A. J. Duncan, F. L. Beyer, G. L. Fiore, S. J. Rowan, C. Weder, *Nature* **2011**, *472*, 334.
[35] G. L. Fiore, S. J. Rowan, C. Weder, *Chem. Soc. Rev.* **2013**, *42*, 7278.
[36] C. Weder, *Nature* **2009**, *459*, 45.
[37] T. F. Scott, A. D. Schneider, W. D. Cook, C. N. Bowman, *Science* **2005**, *308*, 1615.
[38] L. Hu, H. S. Kim, J.-Y. Lee, P. Peumans, Y. Cui. *ACS Nano* **2010**, *4*, 2955.
[39] Y. Sun, B. Mayers, T. Herricks, Y. Xia, *Nano Lett.* **2003**, *3*, 955.
[40] T. Kim, A. Canlier, G. H. Kim, J. Choi, M. Park, S. M. Han. *ACS Appl. Mater. Interfaces* **2013**, *5*, 788.